Central European Journal of Energetic Materials
ISSN 1733-7178; e-ISSN 2353-1843

Cent. Eur. J. Energ. Mater. 2024, *21*(4): 384-409; DOI 10.22211/cejem/195646
Article is available in PDF-format, in colour, at:
https://ipo.lukasiewicz.gov.pl/wydawnictwa/cejem-woluminy/vol-21-nr-4/

Research paper

Development and Testing of a Propulsion System for a Space Robot Platform Operating in 2D Microgravity

Jan Kindracki[1,*)], **Przemysław Paszkiewicz**[1)], **Łukasz Mężyk**[1)], **Tomasz Rybus**[2)], **Karol Seweryn**[2)], **Tomasz Barciński**[2)]

[1)] *Institute of Heat Engineering, Warsaw University of Technology, Nowowowiejska 21/25 Street, 00-665 Warsaw, Poland*

[2)] *Space Research Centre of the Polish Academy of Sciences, Bartycka 18A Street, 00-716 Warsaw, Poland*

* *Email:* Jan.Kindracki@pw.edu.pl

ORCID information:
Kindracki J.: https://orcid.org/0000-0002-3453-7776
Paszkiewicz P.: https://orcid.org/0000-0001-9272-3449
Mężyk Ł.: https://orcid.org/0000-0002-2297-5672
Rybus T.: https://orcid.org/0000-0002-7957-5346
Seweryn K.: https://orcid.org/0000-0002-4372-0900
Barciński T.: https://orcid.org/0000-0001-6840-953X

Abstract: Robotic arms for use aboard satellites continue to attract much research and development interest due to the vast range of potential applications, ranging from satellite servicing to debris removal. The challenges faced relate to the extent of the complexity of the system and the demands made. The Space Research Centre of the Polish Academy of Sciences, in collaboration with the Warsaw University of Technology, was engaged in research aimed at designing and constructing a robotic platform that was equipped with air bearings and operated on a granite table – thereby simulating 2D microgravity conditions. The paper describes the design process of the propulsion system for the platform, which is a new direction for cold-gas thrusters. The specific requirements regarding the propulsion system, solutions for design problems, and the measurement methods and instrumentation

were covered briefly. These were followed by presenting the facility configuration, evaluation methodology, representative results of single-engine performance, and platform-propulsive module integration mechanism. Finally, on-board propulsion test results were presented in which a comparison of two maneuvers was given, namely, the realization of the same trajectory by the platform in two distinct robotic arm configurations

Keywords: cold-gas propulsion, satellite propulsion, microgravity simulator, active debris removal, in-orbit servicing

1 Introduction

On-Orbit Servicing (OOS) and Active Debris Removal (ADR) missions require the ability to perform autonomous capture maneuvers while in Earth orbit. OOS missions aim to prolong commercial and research satellites' operational lifetime, *e.g.* performing in orbit repairs, replacing components or simply refueling [1]. ADR missions are required to prevent the growth of space debris in Low Earth Orbit. Space debris (*e.g.* spent rocket stages, defunct satellites, and collision fragments) poses a real threat to existing satellites. Studies show that the current debris population will increase due to collisions between existing debris, even if no new objects are put into orbit [2]. Removal of large space debris (which increases in number by several items a year) is needed to prevent the growth of the debris population [3].

Orbital capture maneuvers in OOS and ADR missions can be performed by a robotic manipulator mounted on an unmanned satellite (this method is considered in most of the missions proposed, *e.g.* [4-6]). Orbital capture maneuvers are challenging because the manipulator-equipped satellite must approach the target object and move into close proximity to it. Moreover, the motion of the manipulator affects the position and orientation of the satellite. Technologies required to perform orbital capture maneuvers with the use of a manipulator have been under development since the late 1980s, and to date, several technology demonstration missions have been performed to validate these (*e.g.* ETS-VII in 1997 [7], Orbital Express in 2007 [8]). However, many technologies, especially those required to capture an awkward target, are still at an early stage of development [9]. An uncontrolled target object may be tumbling. The e.Deorbit mission proposed in the range of 4 to 22 N in the past by the European Space Agency (ESA) aims to demonstrate ADR capabilities by capturing Envisat and removing it from orbit [10]. As Envisat is tumbling [11] it is proposed that the chaser satellite will use thrusters to synchronize its motion

with the rotational motion of Envisat [12]. Capture will then be performed with a manipulator and dedicated gripper [13]. This type of operation has never been attempted before. Thus, in the context of the planned e.Deorbit missions and other future OOS and ADR missions, a need arises for test beds that can carry out laboratory verification of technologies designed to perform orbital capture of an uncooperative, awkward, tumbling object. Manipulators are used in orbital missions for various purposes. Since the Space Shuttle entered service in 1981 the Shuttle Remote Manipulator System (SRMS) has been used to deploy, maneuver and capture payloads [14]. Several manipulators are operated on the International Space Station (ISS) to assist astronauts in maintaining position [15]. In Europe, the ERA arm was built to support activities on the European module of ISS [16], and in Deutschen Zentrums für Luft- und Raumfahrt (DLR), a 3rd generation of the arm was built [17]. The Space Research Centre of the Polish Academy of Sciences (CBK PAN) is developing the WMS LEMUR robotic arm for future autonomous orbital maneuvers [18].

Microgravity is an aspect of the space environment that is especially difficult to recreate on Earth. Yet, it is important for various devices, particularly manipulators and thrusters, during close proximity operations. Experiments performed in simulated microgravity conditions are needed to test engineering models of the proposed manipulators and thrusters and proposed control algorithms and to validate numerical simulations of the capture maneuver (contact occurring during the orbital capture maneuver is a highly nonlinear phenomenon, and it is difficult to obtain high fidelity models of contact [19]). There are several ways of simulating microgravity conditions on Earth [20]. Planar air-bearing microgravity simulators are especially well suited for validation of technologies related to OOS and ADR missions [21]. Using this approach, the test objects (*e.g.* satellite mock-up equipped with a manipulator) are mounted on planar air bearings, allowing almost frictionless motion in one plane (a friction coefficient of around 10^{-5} can be obtained). Thus, microgravity conditions can be simulated in two dimensions. This limitation is acceptable in many applications. The more notable examples of experiments performed with planar air bearing microgravity simulators include formation flying experiments performed in relation to the SPHERES (Synchronized Position Hold Engage Re-orient Experimental Satellites) program developed at the Massachusetts Institute of Technology [22], experiments related to the proposed Orion mission performed at Stanford University [23] and experiments related to rendezvous between two satellites performed at the DLR Institute of Space Systems [24]. Several very recent studies, *e.g.* [25], focus on controlling a small manipulator-equipped satellite (space robot) during the approach and capture of the target

object and relate directly to work on OOS and ADR missions. Besides robotic systems being used to capture the desired object, the propulsion system selection process is an important issue relating to OOS and ADR missions. Since many mission scenarios consider close approach maneuvers to objects that may be tumbling, it would be necessary for a propulsion system to allow precise position changes and velocity corrections would be necessary.

Many different types of propulsion systems may be used on spacecraft. The types used are cold-gas thrusters and chemical and electric propulsion [26]. The most common options regarding chemical propulsion are liquid bi- and monopropellant thrusters. A single propellant is used in a monopropellant thruster, greatly reducing the system's complexity. The working fluid passes through a catalyst bed, where a rapid, highly exothermal decomposition occurs. The products generated are accelerated in a conventional supersonic nozzle. Hydrazine is the chemical currently employed in the vast majority of cases. While hydrazine undoubtedly displays good performance and high stability, it suffers from a serious drawback: high toxicity [27]. Much effort is being directed into applying alternative "green propellants" [28]. Leading candidates are ammonium dinitramide (ADN), hydroxyl ammonium nitrate (HAN) based propellants [29-32], and highly concentrated hydrogen peroxide (High Test Peroxide, HTP) [33-35]. An additional propellant is used in a bipropellant thruster, making the system more complicated but greatly enhancing performance. Since bipropellant systems are also based on toxic, hypergolic compounds, there is also an increasing interest in developing alternative propellants [36-38]. Cold-gas thrusters are the simplest form of rocket engine. Their main components are a valve and nozzle. Performance is low as only a high-pressure gas is used with these propulsion devices (gas is accelerated in the nozzle). Still, they enjoy major advantages: high reliability, repeatability and precision, simple design, and low cost [39]. Hydrogen, helium, nitrogen, argon, *etc.* may be employed as the working medium [26].

In an electrothermal thruster, the gas is heated before entering the nozzle [40, 41]. Resistojets and arcjets are two representative solutions in this group. Resistojets use a resistively heated element to increase the propellant temperature before the expansion process. In arcjet thrusters, an electric arc is generated in the flow path of the propellant. Other, more sophisticated solutions (not discussed here) include electromagnetic and electrostatic propulsion, which combine magnetic and electrostatic fields [42]. Figure 1 presents schematic views of four thrusters: resistojet, arcjet, monopropellant, and bipropellant.

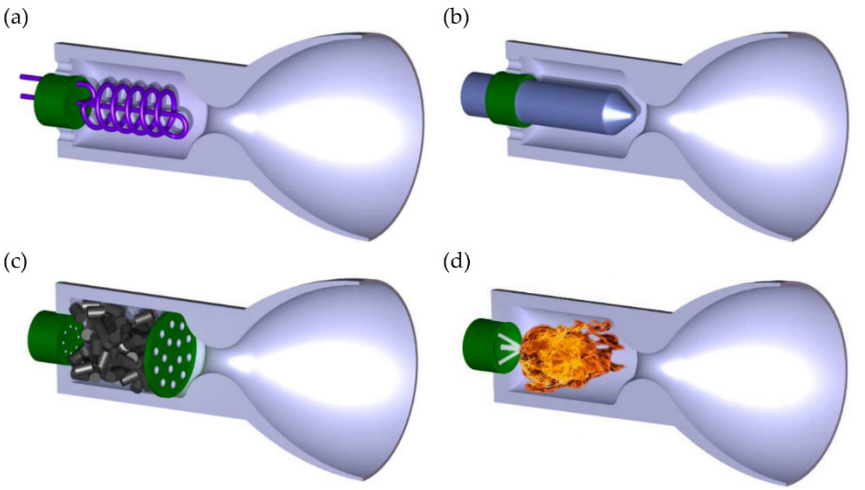

Figure 1. Schematic view of different types of thrusters: resistojet (a), arcjet (b), monopropellant (c) and bipropellant (d) (source of picture: [43])

The project undertaken by CBK PAN in collaboration with Warsaw University of Technology (and several Polish companies) seeks to develop and validate selected technologies required to perform the orbital capture maneuver using a small autonomous space robot equipped with thrusters and a manipulator. Within the framework of this project, a set of experiments in simulated microgravity conditions was performed on a planar air-bearing microgravity simulator at CBK PAN [44]. The following sections will cover the definition of requirements, thruster design, and an explanation of some design details.

2 Definition of Requirements and Control System Implementation

The study selected a 570 kg space robot with a 2.5 m robotic manipulator as a baseline solution. The space robot is smaller than the one proposed in the e.Deorbit mission [10], but analysis showed that the smaller space robot could have numerous applications, including on-orbit servicing of satellites and removal of space debris (smaller than Envisat) from orbit. Due to the limited size of the test facility and the limited loads that can be carried by air bearings, scaled-down mock-ups of real systems had to be used in the experiments. The planar air bearing microgravity simulator has a granite base plate measuring 2×3 m. Thus, a mock-up of the space robot had to be scaled down to fit into this area and

have enough space to demonstrate the capture maneuver (including the approach phase). To obtain the same dynamic behavior of the scaled-down system as the real system, scaling must be performed as per the scaling law [45]:

$$P_s = k^w P \tag{1}$$

where P_s denotes the value after scaling, k is the scaling coefficient, w is the scaling exponent, and P is the value before scaling. Several representative scaling exponents for specific physical properties are shown in Table 1. In contrast, in Table 2, the parameters of the proposed space robot are presented along with the parameters of the scaled-down mock-up of this robot.

Table 1. Physical properties with scaling exponents

Physical property	Scaling exponent	Physical property	Scaling exponent
Distance	1	Inertia	5
Time	1	Velocity	0
Frequency	–1	Acceleration	–1
Force	2	Energy	3
Mass	3	Power	2

Table 2. Scaling of the space robot [46]

Parameter	Real space robot (3D)	Space robot in CBK PAN (2D)
Total mass, m_c [kg]	570	66.16
Mass of the base, m_b [kg]	518.18	60.15
Mass of the manipulator, m_m [kg]	51.82	6.01
Manipulator length, l_m [m]	2.50	1.22
Base inertia, I_b [kg·m^2]	–	2.199
Ratio, m_m/m_b [-]	0.10	0.10
Ratio, m_m/m_c [-]	0.09	0.09
Scaling coefficient, k	–	0.4878

It is important to note that the duration of the experiment is also scaled. The results from a test performed with the scaled-down system can be re-scaled to the full-scale model and used for analysis. The space robot mock-up is shown in Figure 2, while a detailed description of the mock-up can be found in [46]. The main element of the space robot mock-up is the base platform, to which two high-pressure cylinders are attached (one cylinder contains pressurized air

to operate the air bearings, while the other contains gas used by the thrusters). The mock-up also carries batteries, control electronics, and a visual marker the external vision system uses. Additional mass cans are mounted at the bottom of the base platform to adjust the mass and inertia of the mock-up and allow experiments for differently scaled satellites.

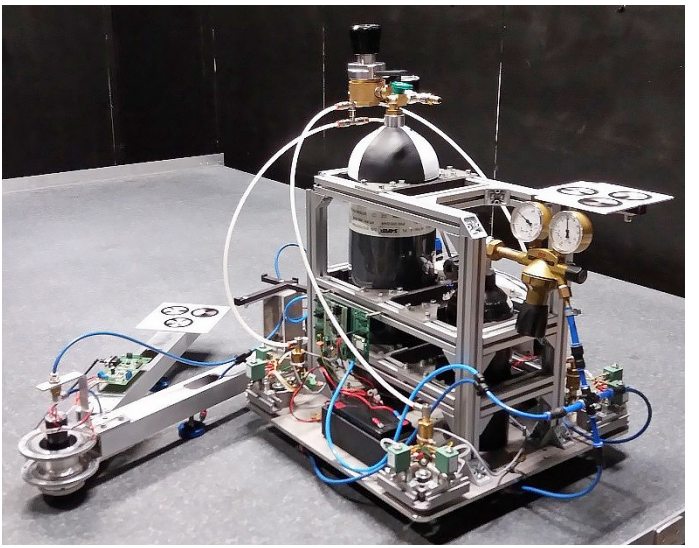

Figure 2. The space robot mock-up

A two DoF manipulator can be mounted on one side of the base platform. In the selected solution, eight thrusters are used to fully control the position and orientation of the space robot mock-up on the test bed. The requirements for the thrusters are based on the proposed mission scenario (capture of an uncontrolled target) and on the scaled-down system's parameters (including the experiment's expected time of around 10-20 s). As found in [47], Reaction Control Systems (RCS) for precise attitude and orbit control of a spacecraft operate with typical thrust in the 4 to 22 N range. The requirement for approx. 1 N thrust was set for the space robot mock-up (approx. mass 68 kg) since it gives 4.2 N for the full-scale system upon rescaling with the chosen scaling coefficient. According to the limits of the test-bed size, the maximum velocity of the mock-up achievable with this thrust is around 0.3 m/s, given the assumption that the motion of the mock-up starts from stationary and is accelerated and decelerated with the use of thrusters only. The estimated duration of the experiment is around 20 s, which satisfies the technical requirements. The control system has to deal with the actuation problem because 8 cold gas thrusters influence only three outputs:

position x, position y, and orientation, since the motion is restricted to one plane. For this purpose, a mapping matrix, $\mathbf{A}^{3x8}$, was formulated, which transforms forces on 8 thrusters to a resultant force and torque. The locations of thrusters on the mock-up are shown in Figure 3.

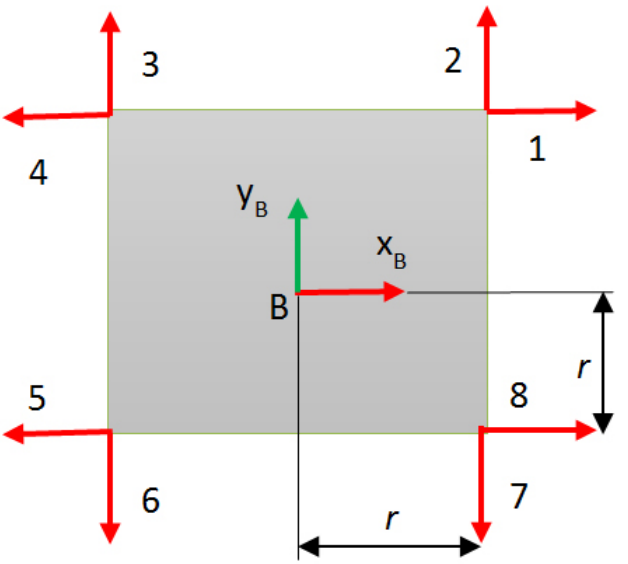

Figure 3. Schematic diagram of the base mock-up with thruster locations and numeration

Point B of the mock-up base is in the geometrical center of the base plate. Each thruster is placed symmetrically with respect to point B at a distance of r = 0.2 m in both the x and y directions. The center of mass of the base is shifted by $x_m = 3.54 \cdot 10^{-4}$ m and $y_m = -1.279 \cdot 10^{-3}$ m from point B. The free-floating system of the base mock-up with 8 thrusters can be described as follows [45]:

$$\begin{bmatrix} F_x \\ F_y \\ \tau_z \end{bmatrix} = \mathbf{A}^{3x8}\mathbf{f} \tag{2}$$

where $\mathbf{f} = [f_1 \ \ldots \ f_8]^T$ are forces acting on the eight cold gas thrusters, as per Figure 3, F_x and F_y are the resultant forces in and direction in the base reference frame (x_B, y_B), τ_z is the torque with respect to axis and $\mathbf{A}^{3x8}$ is the mapping matrix transposing eight forces on cold gas thrusters to resultant force and torque. The mapping matrix is formulated as:

$$\mathbf{A}^{3x8} = \begin{bmatrix} -1 & 0 & (r - y_m) \\ 0 & -1 & (-r + x_m) \\ 0 & -1 & (r + x_m) \\ 1 & 0 & (-r + y_m) \\ 1 & 0 & (r + y_m) \\ 0 & 1 & (-r - x_m) \\ 0 & 1 & (r - x_m) \\ -1 & 0 & (-r - y_m) \end{bmatrix}^T \tag{3}$$

The control of the base is formulated as:

$$\mathbf{f} = \mathbf{A}^{\#} \begin{bmatrix} F_x \\ F_y \\ \tau_z \end{bmatrix} \tag{4}$$

where $\mathbf{A}^{\#}$ is the Moore-Penrose pseudoinverse of the matrix $\mathbf{A}^{3x8}$.

The pseudoinverse operation finds a solution vector with a minimum Euclidean norm among all solutions. The benefit of this is that the desired effect of the control (*e.g.* moving the base to the reference position) is achieved with minimum expense of the gas medium. The pseudoinverse distributes the force equally to the thrusters. This means that to move the base in $+x$ axis in an inertial frame, 4 thrusters are calculated to fire (instead of 2), which is impossible. Instead, the force on the thrusters pointed the right way is doubled, and the other is rejected. The approach proved successful in simulation with an open loop trajectory realization, in which the force and torque were calculated from the reference trajectory.

A control scheme based on a PD controller was chosen for the base with feedback on position and orientation. The force and torque input $[F_x, F_y, \tau_z]^T$ is replaced by three PD controller signals [PD(e_x), PD(e_y), PD(e_θ)], where $e_x = (r_x)_{ref} - r_x$, $e_y = (r_y)_{ref} - r_y$, $e_x = (r_\theta)_{ref} - r_\theta$. The correcting gains in PD controllers are chosen experimentally.

The continuous force signal calculated with pseudoinverse has to be modulated due to the operational ON/OFF thruster mode. The portion of energy given by each thruster can only be controlled by its operational time. Therefore, Pulse Width Modulation (PWM) was implemented to control the thrusters, with the duty cycle calculated as follows:

$$D_i = \frac{f_i}{f_{max}} \cdot 100\% \tag{5}$$

where D_i is the duty cycle on a single thruster [%], f_i is the required force on a single thruster and f_{max} the maximum thruster force.

As in the current approach, a duty cycle cannot be higher than 90%; the reference trajectories have to be designed considering the system's limits and available thruster force.

3 Thruster Design

The assumption was that the deviation between the thruster's theoretical calculations and the experimental results would be acceptable. Hence, the decision was not to use any empirical correction factors when predicting the thruster's performance. It was assumed that the goal thrust is $T = 1$ N and nozzle inlet pressure is 10 bar. Gaseous nitrogen was used as a working medium. Table 3 depicts the values used during the design process.

Table 3. Parameters used for the design process (p_1 is the nozzle inlet pressure, and p_e is the nozzle exit pressure)

Parameter	Value	Unit
Thrust	1	[N]
Pressure ratio across the nozzle, p_1/p_e	10	[-]
Specific impulse (sea level), I_{sp}	542	[m·s^{-1}]

Additionally, it was assumed that the nozzle's convergence and divergence half angles are 22.5° and 15°. It was decided that the nozzle would be manufactured as a separate component and would be screwed into the valve and sealed with an o-ring. A 3D model of the nozzle plus selected dimensions is shown in Figure 4.

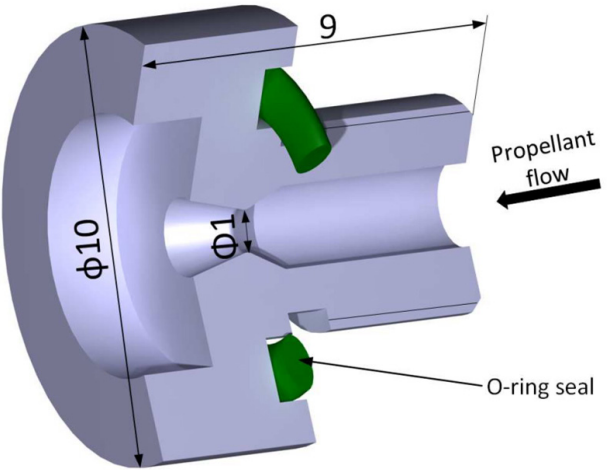

Figure 4. 3D model of the nozzle used in the thruster (dimensions in mm)

4 Platform Propulsion Evaluation

4.1 Test facility and instrumentation

A key objective of this project was to design and build a thruster test facility that would provide a high-performance, low-cost solution. With that assumption in mind, it was decided to use a 300 bar composite tank (among other equipment, including a pressure regulator) and integrate it with a movable table placed on a linear guideway, enabling thrust measurement. The process of filling and evacuating the working fluid in the tank is done using a three-way valve. The valve is connected with an industrial coupling on one side and a pressure regulator on the other. Figure 5 presents a schematic diagram of the facility setup.

Much effort was put into deriving a way of measuring the principal parameters, which enabled a thorough examination of the thruster system. A few measurement sections were introduced to measure the pressure and the temperature of the working fluid. First, the temperature of the gas leaving the pressure regulator is measured. This allows the process of expansion occurring in the vessel to be monitored when the thruster is working. Secondly, absolute pressure is measured upstream of the venturi tube.

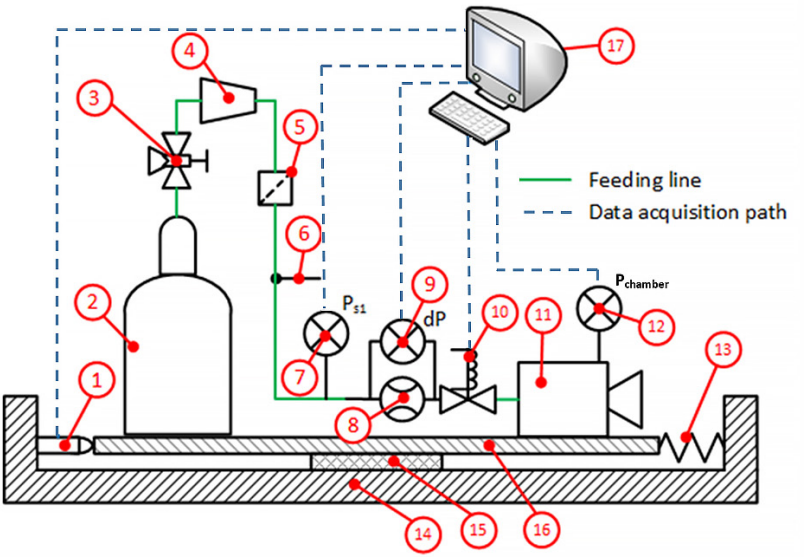

Figure 5. Schematic view of the facility: 1 – force transducer, 2 – high-pressure nitrogen tank, 3 – three-way valve, 4 – pressure regulator, 5 – filter, 6 – thermocouple, 7 – pressure transducer (P_{s1}), 8 – venturi tube, 9 – differential pressure transducer (dP), 10 – solenoid valve, 11 – thruster, 12 – pressure transducer ($P_{chamber}$), 13 – pre-load spring, 14 – supporting structure, 15 – linear guideway, 16 – movable table, 17 – data acquisition system

The self-designed venturi flowmeter was used as a low-cost, high-speed solution for accurate measurement of the mass flow rate of the gas. To measure the pressure difference in the flowmeter, a differential pressure transducer was used (Keller PD-23 series). The pressure port and transducer were placed in the thruster chamber. A Kistler 9205 force transducer was used and placed to measure the thrust value, as shown in Figure 5. The valve is the most important component of a cold-gas thruster. A conventional industrial valve (Parker 201LG series) was thoroughly tested to investigate whether this low-cost component meets project requirements. Before testing, the valve was modified to reduce the system's mass and dead volumes, thereby improving the dynamic characteristics of the thruster. The modification included an additional pressure port to monitor the pressure before the nozzle. Figure 6(a) depicts the first version of the test bench. Research showed the stiffness of the presented design to be insufficient, resulting in poor quality in terms of results and reproducibility. Therefore, it was decided to redesign the supporting structure, the upgraded version shown in Figure 6(b).

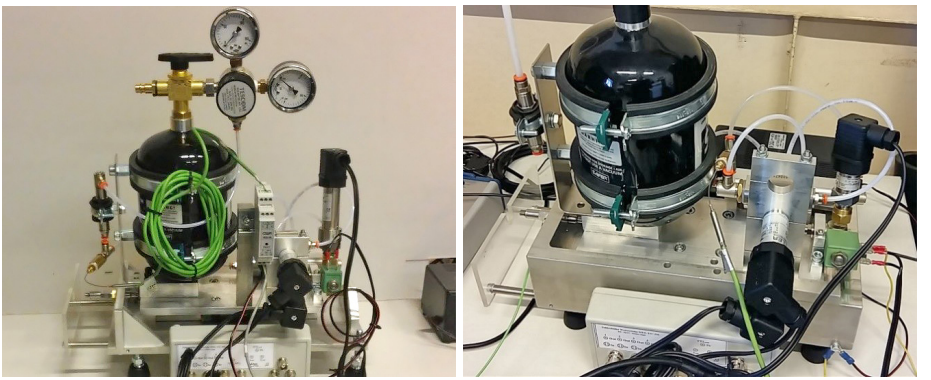

(a) (b)

Figure 6. Thruster test facility (a) before and (b) after modification

4.2 Thruster parameters validation experiments

As mentioned, pressure was measured at several points in the research. Static pressure and temperature upstream of the venturi flowmeter and differential pressure were used for mass flow rate calculation. Thrust was measured directly by the Kistler 9205 sensor using the classical, direct method. A typical experiment lasted about 1000 ms, delivering the output parameters shown in Figure 7.

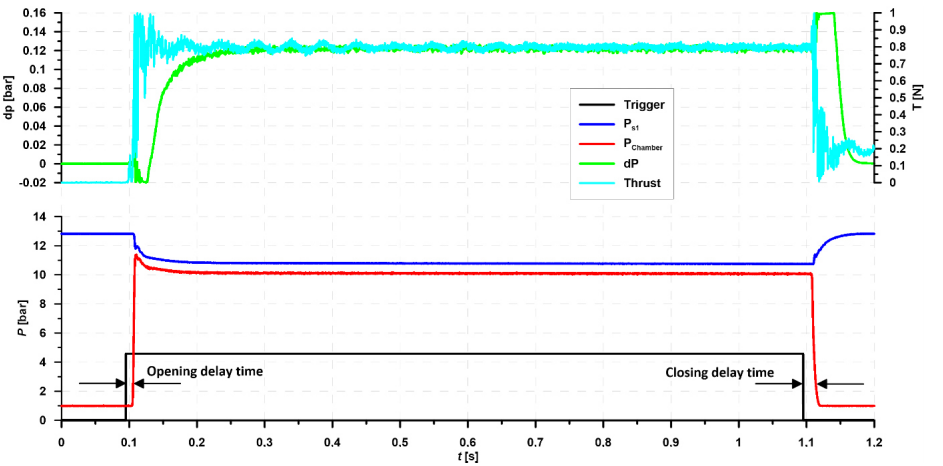

Figure 7. Typical experiment parameters curves

The trigger signal was registered in the experimental data to calculate the valve response time and delays during its opening and closing. The opening delay time is extremely important because the high working frequency is a key

factor in a properly designed thruster. The valve was tested for more than 41.6 h, and about 150,000 full cycles were performed, with pressure in the chamber and duration time of a single experiment being treated as variables. It was proved that a change of parameters, such as the opening time or opening delay, is negligible. Detailed information on the testing procedure and results may be found in [48]. It was found that this thruster achieves 86% of the theoretical thrust value and can operate with a maximum frequency of 35 Hz. Since the main valve of the thruster is a simple on-off valve without any regulation, the only way to control the total impulse is to use the PWM mode [9]. Typical experimental data output recorded during PWM are presented in Figure 8. The trigger which controls the main valve is marked in black. The length of that signal and its frequency are selected in a way that allows the required duty cycle to be obtained. A control algorithm chooses the time shift between single pulses to evenly spread them within the required time of thruster operation. Thrust instabilities are readily visible at the beginning of every pulse for two reasons. The first is the very high gas velocity directly after the valve opening, which is brought about by the large pressure difference (between the gas tank and atmospheric conditions or vacuum – depending on the experiment) on the valve during the inactive state. The second is the electric and electromagnetic interaction between the fields generated by the electromagnetic coil with a piezoelectric force sensor. To calculate mean thrust, the initial range of every measurement, where the vibration has its highest amplitude, is omitted to limit the influence of the instabilities on the final results.

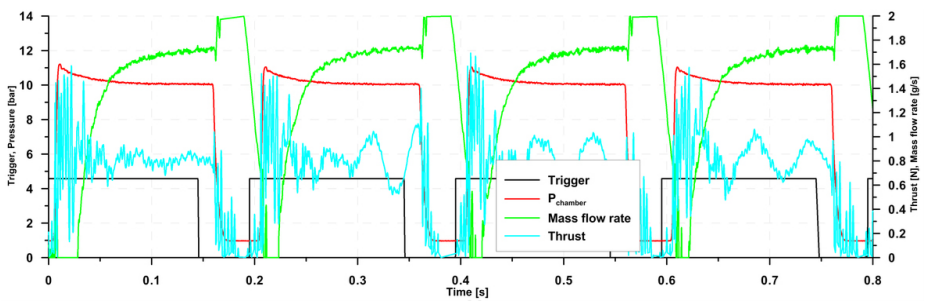

Figure 8. Typical experiment for PWM working mode

As stated earlier, the project's main goal is to deliver a set of thrusters dedicated to moving the robotic platform on a planar air-bearing microgravity simulator. In the proper configuration, eight thrusters may perform translations in a plane of the table (x and y axes) together with rotations around the axis normal to the table (z-axis). After the final version of the thruster was developed, eight pieces were manufactured to be integrated with the platform. Previously, every

one of them was tested on the thrust measurement stand to evaluate the main parameters. The result of this acceptance procedure is shown in Figure 9. The average value of thrust was found to be ±6%. Detailed information on thruster parameter measurement can be found in [48].

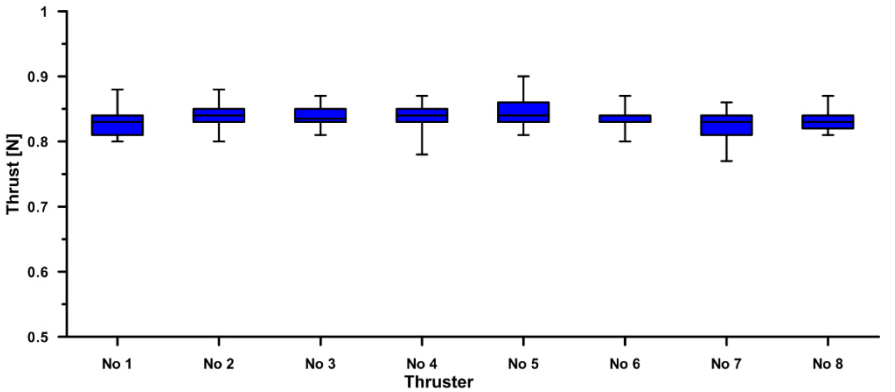

Figure 9. Measured thrust deviation for each thruster

4.3 Propulsive module integration

To simplify the final integration of the propulsion system with a robotic platform and to make this process reproducible and flexible, every couple of engines was integrated into a single module. Each module was designed so that it is possible to rotate it around the axis normal to the platform. It is also possible to move every thruster along the holder axis. Those two features control the direction of the thrust vector generated by each module, allowing calibration with other modules and the platform center of mass to be carried out. Figure 10 shows the computer model of a single propulsive module. The position of the module's rotation axis is fixed using a central pin. Additionally, a 1 μm filter was mounted before every set of engines to reduce the risk of the valve or nozzle becoming blocked with any particles from the high-pressure installation.

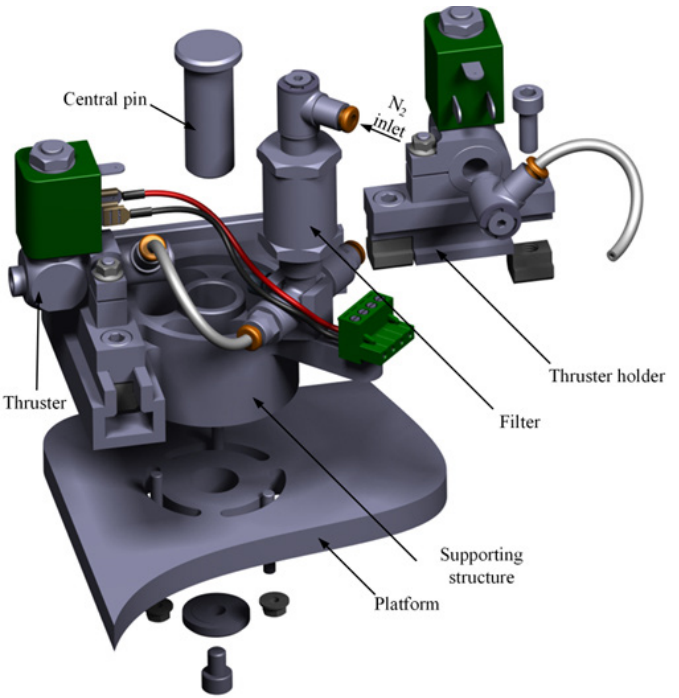

Figure 10. CAD model of the propulsive module with a description of main components

5 On-Board Propulsion Testing

5.1 The microgravity test-bed

The microgravity test bed developed in CBK PAN [44] comprises several components. The key element is a 2×3 m granite table with a leveling system and a flat surface prepared for air bearings. The space robot mock-up has planar air bearings allow for a sliding motion. The test bed was recently upgraded by adding an external vision system provided by OptiNav. It detects visual markers and gives their state (position, orientation) to the control system on the space robot mock-up. The microgravity test bed is shown in Figure 11. The vision system consists of 3 cameras with 5 MPx resolution and a PC with dedicated software, from which the space mock-up is also operated. The robot's commands (*e.g.* trajectory realization) are sent from the PC by USB 2.0 to a triggering device. The device passes the commands to the robot computer using a Bluetooth wireless connection between two STM32 electronic boards

with synchronized processors, one on the triggering device and one on the robot platform. The wire connection was replaced by Bluetooth to minimize the influence of external factors on the mock-up (because a wire connection would hinder its movement). Another function of the triggering device is sending a triggering signal to the cameras with a given frequency.

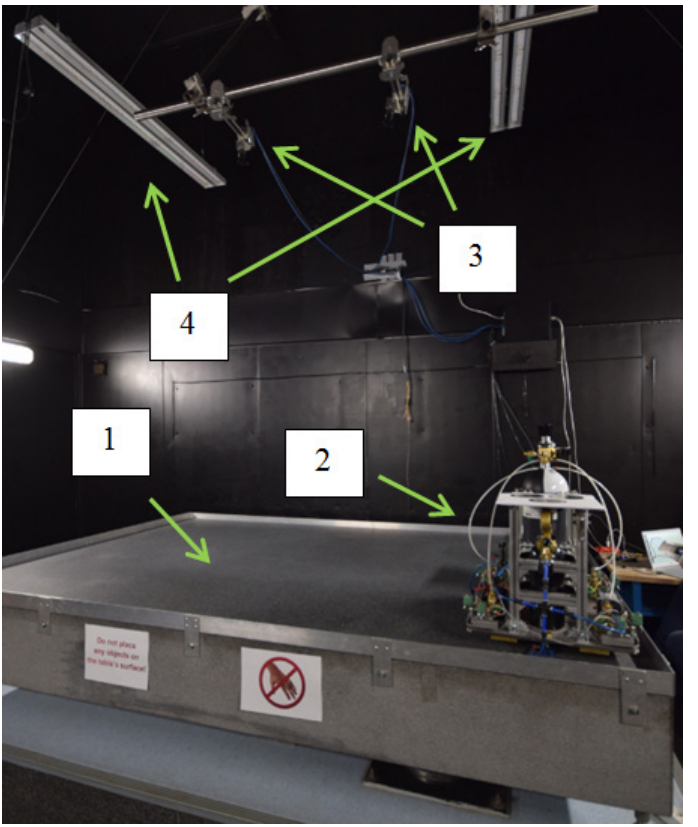

Figure 11. The microgravity test bed: 1 – the air-bearing table, 2 – the space robot mock-up, 3 – vision system cameras, and 4 – the illumination system

The device also sends a unique time tag for every acquired image to the PC, which is then attached to the measurements to locate the time instant of the measurement precisely. The robot control system uses the data concerning the position and orientation of tracked markers from each frame obtained by the vision system to actuate 8 cold gas thrusters. The signal transfer in the test system is shown in Figure 12.

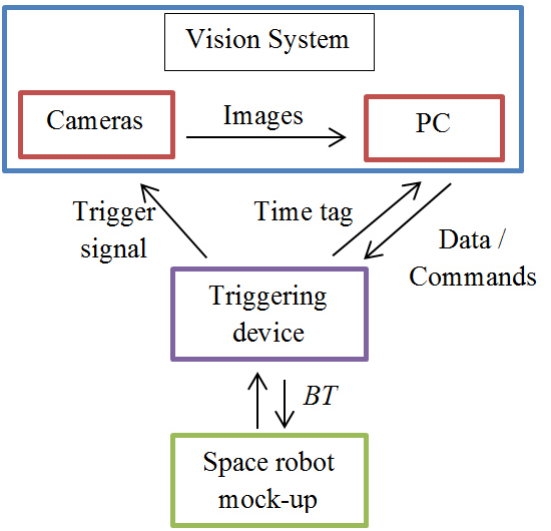

Figure 12. Schematic diagram of the signal transfer in the test system

5.2 Test results

Two exemplary tests in which the 2 DoF manipulator was attached to the base plate were conducted and compared. In both, the base was to perform a linear trajectory in the inertial frame of the granite table, while the manipulator stayed in its initial joint configuration. A visualization of the tests is shown in Figure 13. In the first test, the manipulator was in a deployed position, while in the second it was folded in a position close to the base. It is worth noting that the robot's control system used parameters of the base only. This means that the presence of the manipulator introduced a disturbance to the control system since the mass of the test system increased by 10%.

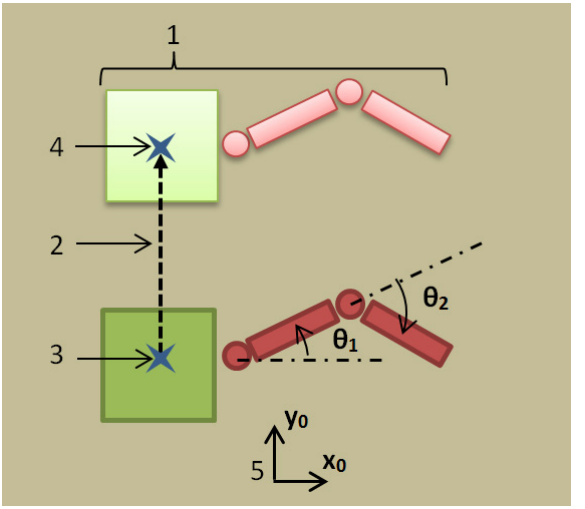

Figure 13. A visualization of the experiment: 1 – space robot, 2 – reference trajectory, 3 – initial position, 4 – final position, 5 – reference frame on the granite table

Moreover, the disturbance would be higher if the manipulator were deployed. At the same time, the position of the center of mass and the inertia of the test system should be subjected to even greater change. Therefore, the primary goal of the test activity was to check if the chosen control approach was valid. In contrast, the secondary goal was to assess the influence of varying unknown parameters of the test system on the quality of trajectory realization in two significantly different cases. During the test, the feedback on the position and orientation of the base from the vision system was sent at a frequency of 5 Hz. The joint positions of the manipulator are shown in Table 4, while the properties of the test system are shown in Table 2.

Table 4. Joint positions of the manipulator in two test cases

Test no.	State of the manipulator	Joint position, θ_1 [deg]	Joint position, θ_2 [deg]
1	deployed	21.5	–32.2
2	folded	107.5	–151.4

The test trajectories were compared with the reference trajectory. Figures 14(a) and 14(b) show trajectory realization along the x and y axes, respectively, and Figure 14(c) shows the orientation of the mock-up. The errors

concerning position and orientation are shown in Figure 14(d). The test results showed successful trajectory realization tasks and applied control schemes. The test led to several important conclusions. It can be seen that the base has some initial position and orientation errors at the start of the experiments. This is because, during the phase preceding the trajectory realization, the base was not placed in the correct initial position by an external system but was moved to it by the thrusters. The error along the *x*-axis, perpendicular to the trajectory, is kept within 50 mm. This error may result from the control system using inaccurate base parameters. The error along the *y-axis* is larger and is kept within 100 mm. Given that a significant overshoot is visible, a higher derivative term in the PD controller is suggested for future experiments. An interesting point is that the trajectory realization is similar in both cases. This means that the applied control scheme is robust to uncertainties. Worthy of consideration is the orientation error, which is positive for the test with the deployed manipulator and negative for the folded manipulator. Intuitively, while moving along the positive *y-axis,* it should be more difficult to maintain the correct orientation for the first case because of higher inertia and higher uncertainty of the position of the center of mass (the position of the center of mass is located further away from the geometrical center of the platform for the first case). The observed behavior derives from the fact that in the folded position, the valve of thruster no. 1 was directed toward the first link of the manipulator. This led to a situation in which part of the thruster no. 1 force acted as an internal force, pushing the base and the manipulator in opposite directions and thereby restricting the effectiveness of orientation correction

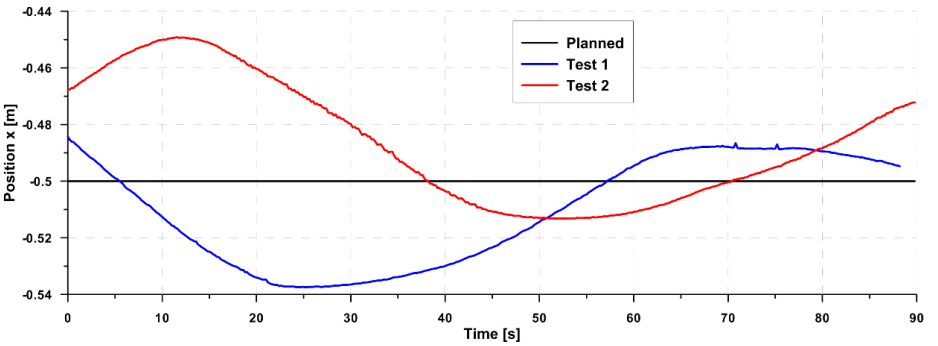

(a)

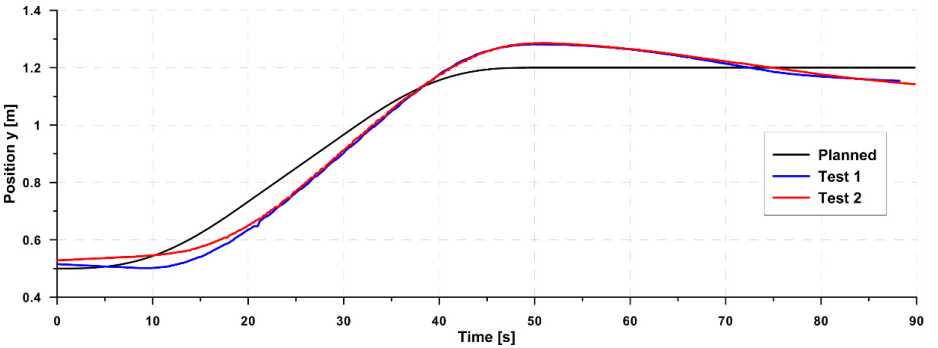

(b)

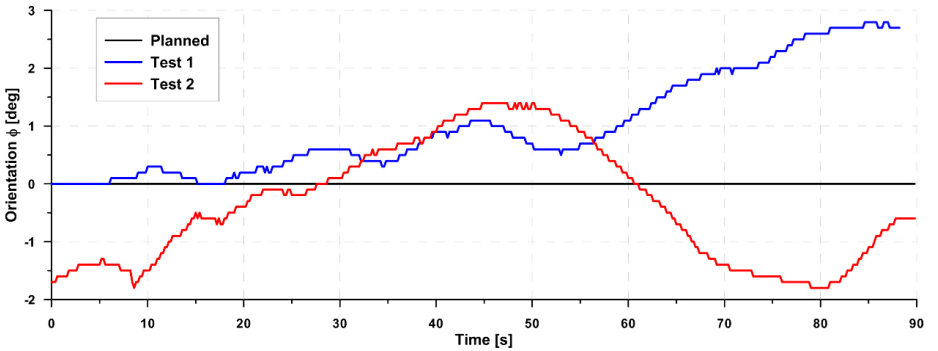

(c)

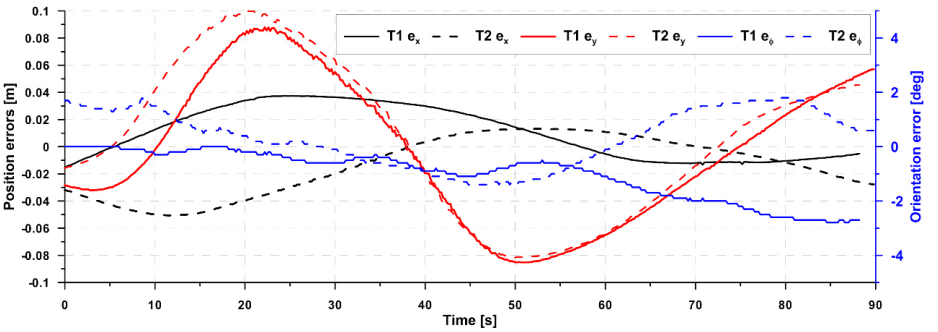

(d)

Figure 14. Trajectory realization: – position in *x* axis (a), – position in *y* axis (b), – orientation (c) and errors of position and orientation (d)

The test described in this paper showed that the system is actuated properly. It is planned to improve the quality of the control and perform more difficult tasks involving manipulator trajectories.

6 Conclusions

- A process of developing a simple propulsion system for a space robot platform is described. The propulsion is based on eight cold gas thrusters, and the platform will be operated on a 2D microgravity test bed.
- Two-dimensional microgravity conditions were obtained using air bearings mounted on the platform and the high-precision granite plate on which it operates.
- The propulsion development process was thoroughly described, including the definition of requirements for thrusters, facilities overview, experimental characterization of thrusters, design descriptions, and final on-board platform testing.
- Final testing was performed using a fully equipped robotic platform for two cases – with deployed and folded robotic arm – and the results were compared. The cold-gas thrusters used commercially available valves modified to meet the project requirements regarding dimensions and working dynamics.
- It was shown that the selected low-cost solution gave satisfactory effects and allowed for thorough system testing.

Acknowledgment

This research was funded by the National Centre for Research and Development, Poland, project No. PBS3/A3/22/2015. The authors would like to thank Jakub Oleś, Kamil Tarenko, and Radosław Moczydłowski for their help in conducting some experiments.

References

[1] Waltz, D. *On-Orbit Servicing of Space Systems*. Kriger Publishing Company, **1993**; ISBN: 089464002X.

[2] Liou, J.C.; Johnson, N.L. Instability of the Present LEO Satellite Populations. *Adv. Sp. Res.* **2008**, *41*: 1046-1053; https://doi.org/10.1016/j.asr.2007.04.081.

[3] Liou, J.C.; Johnson, N.L.; Hill, N.M. Controlling the Growth of Future LEO Debris Populations with Active Debris Removal. *Acta Astronaut.* **2010**, *66*: 648-653; https://doi.org/10.1016/j.actaastro.2009.08.005.

[4] Bischof, B.; Kerstein, L.; Starke, J.; Guenther, H.; Foth, W.; Al, E. ROGER – Robotic Geostationary Orbit Restorter. *Proc. 54th Int. Astronaut. Congr.* **2003**, Bremen, https://doi.org/10.2514/6.IAC-03-IAA.5.2.08.

[5] Del Cura, J.; Saavedra, G.; Sánchez-Maestro, R.; Sebastián, A.; Tarabini, L.; Ortega,

G. Conexpress Orbital Life Extension Vehicle Cx-Olev Gnc. *Proc. 6th Int. ESA Conf. Guid. Navig. Control Syst.* **2006**.

[6] Xu, W.; Liang, B.; Li, C.; Xu, Y. Autonomous Rendezvous and Robotic Capturing of Non-Cooperative Target in Space. *Robotica* **2010**, *28*: 705-718; https://doi.org/10.1017/S0263574709990397.

[7] Oda, M. Summary of NASDA's ETS-VII Robot Satellite Mission. *J. Robot. Mechatronics* **2000**, *12*: 417-424; https://doi.org/10.20965/jrm.2000.p0417.

[8] Ogilvie, A.; Allport, J.; Hannah, M.; Lymer, J. Autonomous Satellite Servicing Using the Orbital Express Demonstration Manipulator System. *Proc. 9th Int. Symp. Artif. Intell. Robot. Autom. Sp.,* **2008**.

[9] Flores-Abad, A.; Ma, O.; Pham, K.; Ulrich, S. A Review of Space Robotics Technologies for On-Orbit Servicing. *Prog. Aerosp. Sci.* **2014**, *68*: 1-26; https://doi.org/10.1016/j.paerosci.2014.03.002.

[10] Biesbroek, R.; Soares, T.; Husing, J.; Innocenti, L. A Design Study for the Safe Removal of a Large Space Debris. *Proc. 6th Eur. Conf. Sp. Debris,* **2013**.

[11] Schildknecht, T.; Krag, H.; Flohrer, T. Determining, Monitoring and Modelling the Attitude Motion of Potential ADR Targets. *Proc. Clean Sp. Ind. Days,* **2016**.

[12] Jaekel, S.; Lampariello, R.; Rackl, W.; Brunner, B.; Porges, O.; Kraemer, E.; Pietras, M.; Ratti, J.; Biesbroek, R. Robotic Aspects and Analyses in the Scope of the e.deorbit Mission Phase B1. *Proc. 14th Symp. Adv. Sp. Technol. Robot. Autom.,* **2017**.

[13] Wieser, M.; Richard, H.; Hausmann, G.; Meyer, J.C.; Jaekel, S.; Lavagna, M.; Biesbroek, R. e.Deorbit Mission: OHB Debris Removal Concepts. *Proc. 13th Symp. Adv. Sp. Technol. Robot. Autom.,* **2015**.

[14] Jenkins, D.R. *Space Shuttle: The History of the National Space Transportation System, The First 100 Missions.* 3rd ed., **2001**.

[15] Stieber, M.E.; Hunter, D.G.; Abramovici, A. Overview of the Mobile Servicing System for the International Space Station. *Proc. 5th i-SAIRAS Conf.*, Noordwijk, Netherlands, **1999**.

[16] Boumans, R.; Heemskerk, C. The European Robotic Arm for the International Space Station. *Rob. Auton. Syst.* **1998**, *23*: 17-27; https://doi.org/10.1016/S0921-8890(97)00054-7.

[17] Albu-Schäffer, A. *Control of Robots with Elastic Joints Using the DLR Lightweight Arms as an Example.* (in German) Doctoral Thesis, Technische Universisät München, Munich, Germany, **2002**; https://api.semanticscholar.org/CorpusID:171419779/.

[18] Seweryn, K.; Grassmann, K.; Rutkowski, K.; Rybus, T.; Wawrzaszek, R. Design and Development of Two Manipulators as a Key Element of a Space Robot Testing Facility. *Arch. Mech. Eng.* **2015**, *62*(3): 377-394; https://doi.org/10.1515/meceng-2015-0022.

[19] Oleś, J.; Seweryn, K.; Surowiec, M.; Wojtyra, M.; Pietras, M.; Scheper, M. Testing and Simulation of Contact During On-Orbit Operations. *Proc. 14th Symp. Adv. Sp. Technol. Robot. Autom.,* **2017**.

[20] Menon, C.; Busolo, S.; Cocuzza, S.; Aboudan, A.; Bulgarelli, A.; Bettanini, C.; Marchesi, M.; Angrilli, F. Issues and Solutions for Testing Free-Flying Robots. *Acta Astronaut.* **2007**, *60*: 957-965; https://doi.org/10.1016/j.actaastro.2006.11.014.
[21] Rybus, T.; Seweryn, K. Planar Air-bearing Microgravity Simulators: Review of Applications, Existing Solutions and Design Parameters. *Acta Astronaut.* **2016**, *120*: 239-259; https://doi.org/10.1016/j.actaastro.2015.12.018.
[22] Andrade, C.; Ramirez-Mendoza, R.; Giacoman-Zarzar, M.; Morales, R.; Fejric, A.; Saenz-Otero, A.; Miller, D.W. Robust Control Applied Towards Rendezvous and Docking. *Proc. Eur. Control Conf.,* **2009**, pp. 1854-1859; https://doi.org/10.23919/ECC.2009.7074673.
[23] Robertson, A.; Inalhan, G.; How, J. Spacecraft Formation Flying Control Design for the Orion Mission. *Proc. Guidance, Navigation, and Control Conf. and Exhibit*, Reston, Virigina, **1999**, pp. 1562-1575.
[24] Di Mauro, G.; Schlotterer, M.; Theil, S.; Lavagna, M. Experimental Implementation of SDRE Method for Autonomous Rendezvous and Docking Maneuvering. *Proc. 5th Int. Conf. Spacecr. Form. Fly. Mission. Technol.,* **2013**, pp. 1-15.
[25] Virgili Llop, J.; Drew, J.; Zappulla, R.; Romano, M. Autonomous Capture of a Resident Space Object by a Spacecraft with a Robotic Manipulator: Analysis, Simulation and Experiments. *Proc. AIAA/AAS Astrodynamics Specialist Conf.*, Reston, Virginia, **2016**, pp. 1-18.
[26] Sutton, G.; Biblarz, O. *Rocket Propulsion Elements.* 8th Ed., John Wiley & Sons Inc., **2010**; ISBN: 0471326429.
[27] Rarata, G.; Rokicka, K.; Surmacz, P. Hydrogen Peroxide as a High Energy Compound Optimal for Propulsive Applications. *Cent. Eur. J. Energ. Mater.* **2016**, *13*: 778-790; https://doi.org/10.22211/cejem/65005.
[28] Gohardani, A.S.; Stanojev, J.; Demairé, A.; An, K.; Persson, M.; Wingborg, N.; Nilsson, C. Green Space Propulsion: Opportunities and Prospects. *Prog. Aerosp. Sci.* **2014**, *71*: 128-149; https://doi.org/10.1016/j.paerosci.2014.08.001.
[29] Chen, J.; Li, G.; Zhang, T.; Wang, M.; Yu, Y. Experimental Investigation of the Catalytic Decomposition and Combustion Characteristics of a Non-Toxic Ammonium Dinitramide (ADN)-based Monopropellant Thruster. *Acta Astronaut.* **2016**, *129*: 367-373; https://doi.org/10.1016/j.actaastro.2016.09.027.
[30] Hwan, C.; Wook, S.; June, S. Experimental Investigation of Decomposition and Evaporation Characteristics of HAN-based Monopropellants. *Combust. Flame* **2014**, *161*: 1109-1116; https://doi.org/10.1016/j.combustflame.2013.09.026.
[31] Amrousse, R.; Hori, K.; Fetimi, W.; Farhat, K. Applied Catalysis B: Environmental HAN and ADN as Liquid Ionic Monopropellants: Thermal and Catalytic Decomposition Processes. *Applied Catal. B, Environ.* **2012**, *127*: 121-128; https://doi.org/10.1016/j.apcatb.2012.08.009.
[32] Yu, Y.S.; Li, G.X.; Zhang, T.; Chen, J.; Wang, M. Effects of Catalyst-bed's Structure Parameters on Decomposition and Combustion Characteristics of an Ammonium Dinitramide (ADN)-based Thruster. *Energy Convers. Manag.* **2015**, *106*: 566-575; https://doi.org/10.1016/j.enconman.2015.09.036.

[33] Rarata, G.; Florczuk, W.; Smetek, J. Research on Preparation and Propulsive Applications of Highly Concentrated Hydrogen Peroxide. *J. Aerosp. Sci. Technol.* **2016**, *1*: 42-47; https://doi.org/10.17265/2332-8258/2016.01.006.
[34] Rarata, G.; Rokicka, K. The Manganese Oxides Decomposition Catalysts for Highly Concentrated Hydrogen Peroxide. *Trans. Inst. Aviat.* **2015**, *240*: 49-57; https://doi.org/10.5604/05096669.1194985.
[35] Surmacz, P.; Kostecki, M.; Gut, Z.; Olszyna, A. Aluminum Oxide - Supported Manganese Oxide Catalyst for a 98% Hydrogen Peroxide Thruster. *J. Propuls. Power* **2019**, *35*: 614-623; https://doi.org/10.2514/1.B37359.
[36] Okninski, A.; Bartkowiak, B.; Sobczak, K.; Kublik, D.; Surmacz, P.; Rarata, G.; Marciniak, B.; Wolanski, P. Development of a Small Green Bipropellant Rocket Engine Using Hydrogen Peroxide as Oxidizer. *Proc. 50th AIAA/ASME/SAE/ASEE Jt. Propuls. Conf.* **2014**, pp. 1-10; https://doi.org/10.2514/6.2014-3592.
[37] Kang, H.; Jang, D.; Kwon, S. Demonstration of 500 N Scale Bipropellant Thruster Using Non-Toxic Hypergolic Fuel and Hydrogen Peroxide. *Aerosp. Sci. Technol.* **2016**, *49*: 209-214; https://doi.org/10.1016/j.flowmeasinst.2011.05.001.
[38] Kang, H.; Kwon, S. Green Hypergolic Combination: Diethylenetriamine-based Fuel and Hydrogen Peroxide. *Acta Astronaut.* **2017**, *137*: 25-30; https://doi.org/10.1016/j.actaastro.2017.04.009.
[39] Nguyen, H.; Köhler, J.; Stenmark, L. The Merits of Cold Gas Micropropulsion in State-of-the-Art Space Missions. *Proc. 34th COSPAR Scientific Assembly, The Second World Space Congress,* Houston, US-TX, **2002**.
[40] Gibbon, D.; Baker, A.; Coxhill, I.; Sir, P.; Sweeting, M. The Development of a Family of Resistojet Thruster Propulsion Systems for Small Spacecraft. *Proc. 17th Annu. AIAA/USU Small Satell. Conf.,* **2003**, pp. 1-9.
[41] Kindracki, J.; Paszkiewicz, P.; Mężyk, Ł. Resistojet Thruster with Supercapacitor Power Source – Design and Experimental Research. *Aerosp. Sci. Technol.* **2019**, *92*: 847-857; https://doi.org/10.1016/j.ast.2019.07.010.
[42] Lemmer, K. Propulsion for CubeSats. *Acta Astronaut.* **2017**, *134*: 231-243; https://doi.org/10.1016/j.actaastro.2017.01.048.
[43] Paszkiewicz P. *Experimental Characterization of a sub-Newton Electrothermal Thruster Using 98% Hydrogen Peroxide*. Doctoral Thesis, Warsaw University of Technology, Warsaw, **2024**.
[44] Rybus, T.; Nicolau-Kukliński, J.; Seweryn, K.; Barciński, T.; Ciesielska, M.; Grassmann, K.; Grygorczuk, J.; Karczewski, M.; Kowalski, M.; Krzewski, M.; Kuciński, T.; Lisowski, J.; Przybyła, R.; Skup, K.; Szewczyk, T.; Wawrzaszek, R. New Planar Air-bearing Microgravity Simulator for Verification of Space Robotics Numerical Simulations and Control Algorithms. *Proc. 12th Symp. Adv. Sp. Technol. Robot. Autom. 'ASTRA 2013'*, **2013**, p. 8.
[45] Dexler, K.E. *Nanosystems: Molecular Machinery, Manufacturing and Computation.* Wiley, **1992**; ISBN: 978-0-471-57518-4.
[46] Oleś, J.; Kindracki, J.; Rybus, T.; Mężyk, Ł.; Paszkiewicz, P.; Moczydłowski, R.; Barciński, T.; Seweryn, K.; Wolański, P. A 2D Microgravity Test Bed for the

Validation of Space Robot Control Algorithms. *J. Autom. Mob. Robot. Intell. Syst.* **2017**, *11*: 95-104; https://doi.org/10.14313/JAMRIS_2-2017/21.
[47] Zandenberg, B.T.C. *Modern Liquid Propellant Rocket Engines, 2000 Outlook.* Delft University of Technology, **2014**; https://doi.org/10.13140/2.1.4640.0003.
[48] Kindracki, J.; Tur, K.; Paszkiewicz, P.; Mężyk, Ł.; Boruc, Ł.; Wolański, P. Experimental Research on Low-Cost Cold Gas Propulsion for a Space Robot Platform. *Aerosp. Sci. Technol.* **2017**, *62*: 148-157; https://doi.org/10.1016/j.ast.2016.12.001.

Contribution:

Kindracki J.: foundations, methods, performing the experimental part, other contributions to the publication
Paszkiewicz P.: performing the experimental part, other contributions to the publication
Mężyk Ł.: methods, performing the experimental part, other contributions to the publication
Rybus T.: performing the experimental part, performing statistical analysis
Seweryn K.: foundations, methods, other contributions to the publication
Barciński T.: methods, performing the experimental part

Received: May 9, 2024
Revised: November 6, 2024
First published online: December 5, 2024